THE JOURNAL OF PHYSICAL CHEMISTRY LETTERS
A JOURNAL OF THE AMERICAN CHEMICAL SOCIETY

pubs.acs.org/JPCL

Letter

Enhanced Near-Infrared Emission from Carbon Dots by Surface Deprotonation

Enshan Liu,[#] Tao Liang,[#] Elena V. Ushakova, Bingzhe Wang, Bohan Zhang, Huiqun Zhou, Guichuan Xing, Chunming Wang, Zikang Tang,* Songnan Qu,* and Andrey L. Rogach

Cite This: *J. Phys. Chem. Lett.* 2021, 12, 604–611

Read Online

ACCESS | Metrics & More | Article Recommendations | Supporting Information

ABSTRACT: Carbon dots (CDs) with efficient excitation and emission in deep-red/near-infrared (NIR) spectral range are important for bioimaging applications. Herein, we develop a simple and effective method to significantly enhance both the absorption and emission of CDs in deep-red/NIR by suppressing nonradiative charge recombination via deprotonation of the CD surface. As compared to aqueous solutions at room temperature, NIR emission of CDs in *N*,*N*-dimethylformamide and glycerol experience a 50- and 70-fold increase at −20 °C, respectively, due to enhanced deprotonation ability and viscosity. On the basis of the adjustable NIR fluorescence intensity of CDs, multilevel data encryption in the NIR region is realized by controlling the humidity and the temperature of a CD-ink stamped paper.

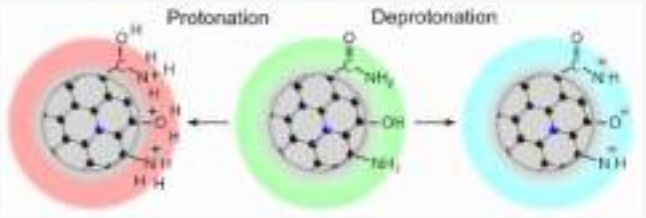

Owing to their attractive optical properties, low cost and biocompatibility, luminescent carbon dots (CDs) have emerged as promising light-emitting materials for various applications such as optoelectronics,[1] photocatalysis,[2] biosensing and bioimaging.[3,4] There have been a lot of reports on CDs with a high photoluminescence quantum yield (PLQY) in the visible spectral region.[1,2,4] Longer wavelength emission in deep-red and near-infrared (NIR) spectral regions are essential for *in vivo* biological imaging, where both tissue autofluorescence and light scattering are minimized, thus improving both imaging contrast and spatial resolution.[5,6] Several groups have reported on CDs with a deep-red and/or NIR emissions, which were excited by light in the green spectral region.[7−9] Heteroatom doping, size control, surface engineering, and control of the chemical environment of CDs were used to modulate absorption bands and NIR emission of CDs. Bi et al. have reported a full-range UV−Vis−NIR emissive CDs by performing F and N codoping;[10] their optimum excitation wavelength was around 550 nm with PLQY of 9.8%. Chao et al. synthesized CDs from o-phenylenediamine through a one-step hydrothermal treatment, which showed multicolor emission with an excitation-independent behavior in different solvents.[11] Our group realized full-color emissive CDs by employing three different solvents, where the emission color was correlated to the CD size.[12] We have also demonstrated NIR absorption and enhanced NIR emission of CDs which has been realized through the surface adsorption of electron-acceptor groups.[13] However, there is still a lack of efficient synthetic methods to move the main absorption band of CDs to deep-red or NIR regions and to realize an efficient deep-red or NIR light excited NIR emission. Furthermore, most of the reported CDs with deep-red or NIR absorption exhibited high photothermal conversion efficiency, leading to low PLQY in the NIR region.[5,14−16] Therefore, it is of primary importance to study and understand the factors affecting the PL emission and the photothermal conversion of CDs in the deep-red/NIR region, in order to design CDs with enhanced emission in this spectral range, and to suppress the energy losses in the samples. It is known that the surface of CDs often contains abundant − OH groups, but there were only a few studies concerning the impacts of the protonation process at CD surface on their energy structure.[17]

Recently, we reported the synthesis of NIR emissive CDs through a solvothermal reaction in dimethyl sulfoxide (DMSO) from two common precursors citric acid and urea, which exhibited a dominant absorption band at 605 nm with a shoulder at 650 nm.[5] Under 655 nm excitation, the aqueous solution of these CDs showed a NIR emission peak at 720 nm with a very low PLQY of 0.2%. In this work, we report a simple and effective method to significantly enhance both the absorption and emission of these CDs in deep-red/NIR region by suppressing nonradiative charge recombination via deprotonation of the CD surface, which has been accomplished by changing the solvent deprotonation ability and viscosity. The emerged dominant absorption band at 650 nm and enhanced NIR emission with PLQY reaching up to 4%

Received: November 12, 2020
Accepted: December 23, 2020
Published: December 31, 2020

https://dx.doi.org/10.1021/acs.jpclett.0c03383
J. Phys. Chem. Lett. 2021, 12, 604−611

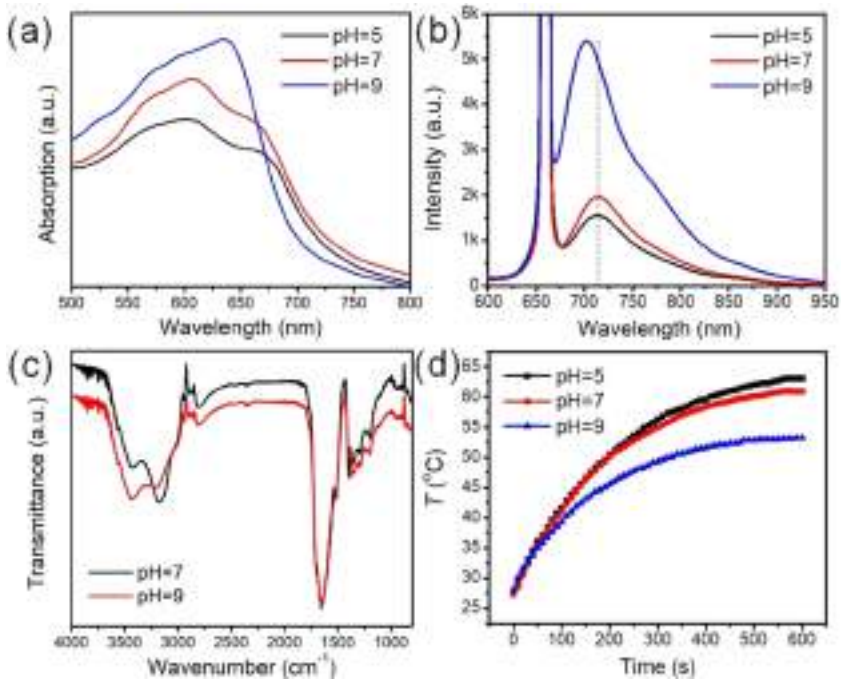

Figure 1. (a) Absorption and (b) PL spectra (excitation at 655 nm) of dilute aqueous solutions of CDs at different pH values (concentration: 50 ppm). The dashed line in (b) shows the position of the PL peak in H_2O at pH = 7. (c) FT-IR spectra of CDs at different pH values. (d) Temperature evolutions of the aqueous solutions of CDs (100 $\mu g \cdot mL^{-1}$) at different pH values under 655 nm laser irradiation at a power density of $1W \cdot cm^{-2}$.

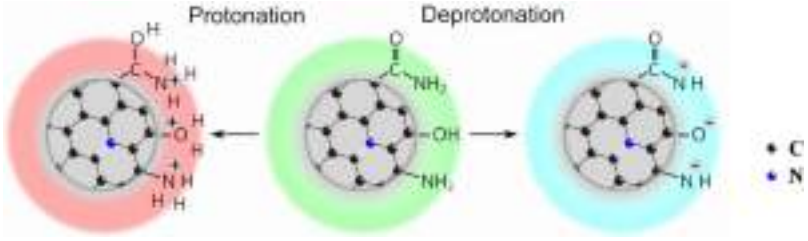

Figure 2. Schematic illustration of the protonation/deprotonation of the CD surface.

and 6% were detected in the CDs glycerol and DMSO solutions at room temperature, respectively. Compared to CD aqueous solution at room temperature, a 50- and 70-fold increase of the NIR emission has been observed for the CDs in N, N-dimethylformamide (DMF) and glycerol solutions at −20 °C, respectively. Based on the environment controllable NIR emission of CDs, multilevel fluorescence encryption was realized by changing the humidity and temperature in the CD-ink stamped paper.

CDs were synthesized according to the previously published procedure, from citric acid and urea via the solvothermal method in DMSO.[5] As demonstrated by X-ray photoelectron spectroscopy (XPS) and Fourier-transform infrared (FT-IR) measurements, these CDs contained hydroxyl, amide, carbonyl, and amine groups at the surface, which are sensitive to pH in aqueous solution due to the protonation/deprotonation processes. As the protonation and deprotonation can increase or decrease the population of the -NH_2 and −OH groups at the CD surface, respectively, potential changes of optical properties of CDs in dilute aqueous solutions at different pH values were tested. Figure 1a and Figure 1b show absorption and PL spectra (at 655 nm excitation) of CDs in aqueous solutions at three different pH values of 5, 7, and 9. In a neutral aqueous solution, CDs exhibit the main absorption band at 605 nm with a shoulder band at 665 nm, and a NIR emission peaked at 715 at 655 nm excitation. In acidic aqueous solution, the shape of the absorption spectrum of the CDs is nearly the same, while the intensities of both the main absorption band and NIR emission are weakened. In contrast, in alkaline aqueous solution, the absorption intensity of the CDs is increased and the main absorption band becomes red-shifted to 645 nm, while the NIR emission is also enhanced but slightly (~10 nm) blue-shifted. To further verify the pH effect on the CD surface chemical groups, FT-IR spectra were measured on samples obtained by freeze-drying of CD aqueous solutions at pH = 7 and pH = 9. As shown in Figure 1c, the broad band at 3000−3500 cm^{-1} consists of 2 peaks at about 3430 and 3200 cm^{-1}, which can be assigned to ν (O−H) and ν (N−H) vibrations in the aromatic ring, respectively. The intense and broad peak at around 1650 cm^{-1} can be attributed to the amide group at the surface, and ν (C−N) and ν (C−C) vibrations in the aromatic ring. Compared to CDs at pH = 7, the absorption band of CDs at pH = 9 at 3430 cm^{-1} is increased, while the band at 3200 cm^{-1} is decreased, suggesting that the increase of pH results in deprotonation of CD surface which in turn leads to improvement of the PL signal. As shown

https://dx.doi.org/10.1021/acs.jpclett.0c03383
J. Phys. Chem. Lett. 2021, 12, 604−611

Table 1. Optical Characteristics of CDs in Dilute H_2O, Glycerol, Ethanol, DMSO, and DMF Solvents[a]

solvent	protic/aprotic	relative polarity	abs peak (nm)	PL peak (nm)	PL lifetime (ns)	PLQY (%)	viscosity (10^{-3} Pa·s, 25 °C)
H_2O		1	665	710	0.80	0.2	0.89
glycerol	protic	0.812	670	705	1.28	4.0	934
ethanol	protic	0.654	660	690	1.78	2.2	1.07
DMSO	aprotic	0.444	670	685	2.32	5.9	1.99
DMF	aprotic	0.386	665	685	2.42	4.9	0.79

[a]The mass concentration of the CDs in all measurements were 0.05 mg/mL.

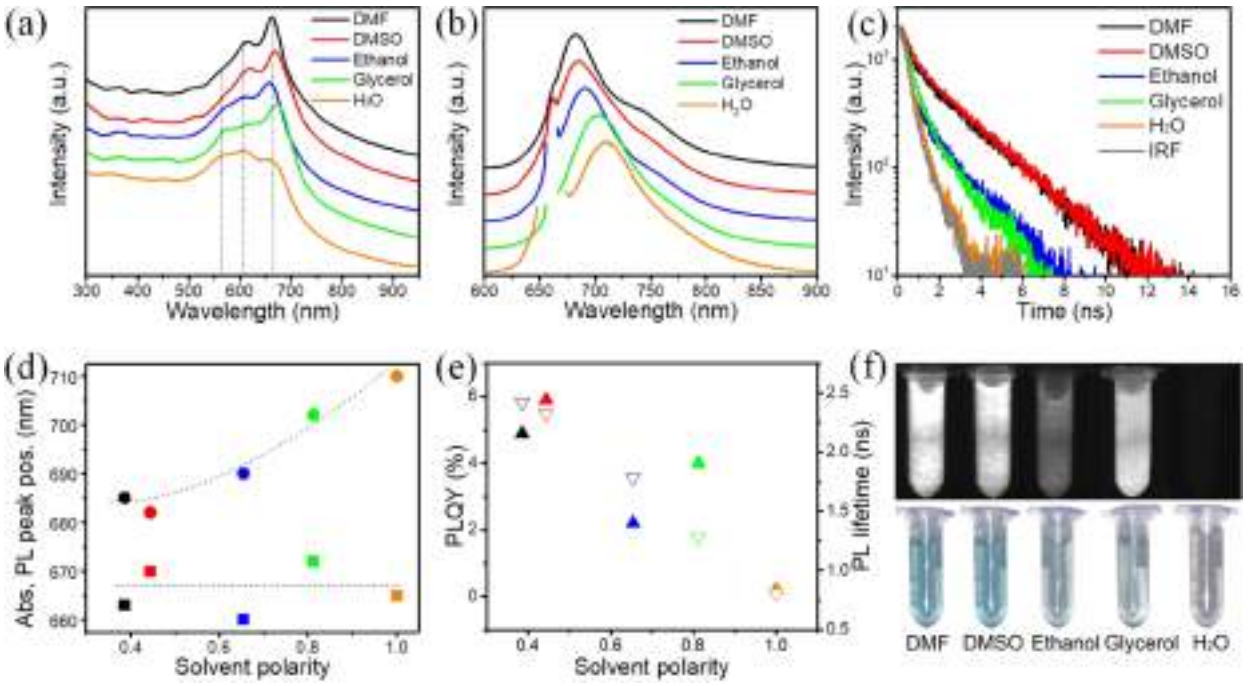

Figure 3. (a) UV−visible absorption and (b) PL spectra (excited at 655 nm) of CDs in H_2O, glycerol, ethanol, DMSO, and DMF solvents (concentration: 50 ppm). The gap in the PL spectra of ethanol, glycerol, and H_2O) at 650−670 is due to subtraction of the peak from the excitation source. (c) PL decay curves of CDs in H_2O, glycerol, ethanol, DMSO, and DMF, monitored at 700 nm under 640 nm excitation. IRF stays for instrumental response function. (d) Peak positions of the lowest energy absorption (solid squares) and PL (solid circles) of CDs derived from the data provided in frames (a) and (b), with the same color coding for different solvents. The dashed lines are guides for the eye. (e) PLQY (solid triangles) and PL lifetimes (hollow triangles) of CDs plotted vs the relative solvent polarity, the color coding indicate the respective solvent. (f) NIR fluorescence images (under 655 nm excitation, top) and bright field images (bottom) under daylight of CDs in different solvents.

in Figure 2, at acidic pH, the protonation renders the surface of the CDs with less electron-rich groups, while at the basic pH, the deprotonation process leads to the appearance of more electron-rich surface groups.

As was reported in our previous work, the CDs exhibit high photothermal conversion efficiency in neutral aqueous solution, equal to 59%.[5] The photothermal behavior of CDs in aqueous solutions at different pH values were tested and are summarized in Figure 1d. Under 655 nm laser irradiation at a power density of 1 W·cm^{-2} for 10 min, the final temperature of the 100 ppm of CD aqueous solutions at pH equal 5, 7, and 9 have increased from 27 °C to 63, 61, and 53 °C, respectively, indicating decreased photothermal performance with increasing pH. Considering that the main difference of the CD surface at low and high pH values is the population of the amine, carbonyl groups, and H-bonding, it can be inferred that the decreased H-bonding and deprotonation process of CDs at basic pH results in a lower vibrational energy dissipation, which might be the reason for the enhanced NIR emission.

To further reveal the details of interaction of CDs with the different chemical environments, their optical responses were measured in a set of solvents which differ in deprotonation ability, polarity, and viscosity. The data obtained, alongside with the characteristics of the solvents used, are summarized in Table 1. Panels a and b of Figure 3 show absorption and emission spectra of CDs in different solvents at room temperature. Upon changing solvents from H_2O to DMF, both absorption and PL spectra become better structured, which agrees with the observations for the organic dyes, where both the H-bonding and the protonation of the luminophore's groups may cause broadening and blurring of peaks in the absorption and emission spectra.[18] In protic solvents (glycerol and ethanol), the PLQYs of CDs reach 2.2% and 4.0%, respectively, which is more than 20-fold enhancement of their PLQY in H_2O (0.2%). Both DMF and DMSO are aprotic solvents with good deprotonation ability due to their electron-acceptor groups C═O/S═O; the NIR emission of CDs in these two solvents is further enhanced, with PLQYs reaching 4.9% in DMF and 5.9% in DMSO. The PL decay curves for NIR emission of the CDs in different solvents monitored at 700 nm under 640 nm excitation are shown in Figure 3c. The average PL lifetime of CDs in aprotic solvents (DMF and DMSO) is longer than in protic solvents (ethanol and glycerol), which well coincides with the observation that

https://dx.doi.org/10.1021/acs.jpclett.0c03383
J. Phys. Chem. Lett. 2021, 12, 604−611

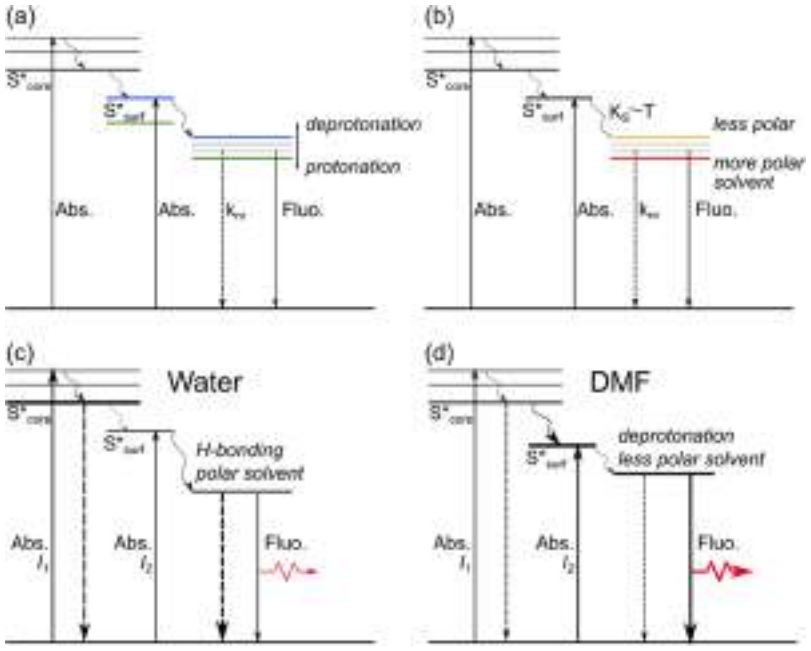

Figure 4. Proposed energy diagrams of the CDs: (a) during protonation/deprotonation, (b) with the effect of solvent polarity, (c) in H_2O solution, and (d) in DMF solution. S^*_{core} and S^*_{surf} are energy states corresponding of the core (I_1 in Figure 5a–c) and surface (I_2 in Figure 5a–c) absorption bands, respectively. Abs, Fluo, and k_{nr} designate absorption, emission, and nonradiative dissipation of energy, respectively, with the last shown by dashed lines. The internal conversion is shown by wavy lines. The thickness of the lines corresponds to the anticipated intensity of the transitions.

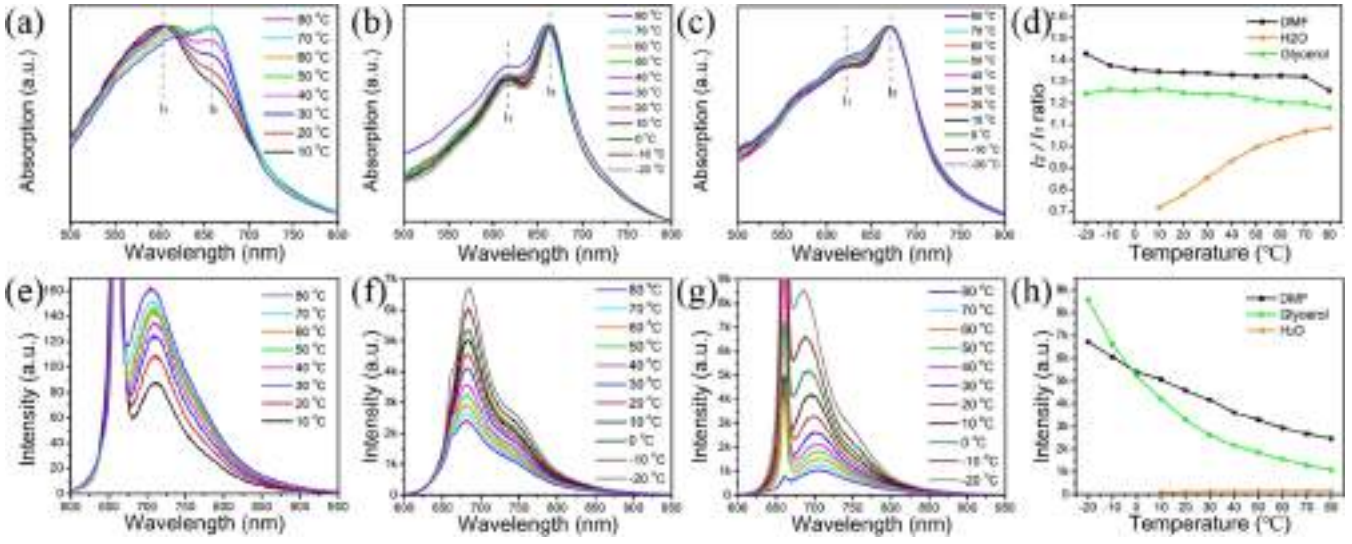

Figure 5. Absorption spectra of CDs (50 ppm concentration) in (a) H_2O, (b) DMF, and (c) glycerol at different temperatures. Dashed lines indicate the positions of two major absorption peaks (I_1 at ~605 nm and I_2 at ~665 nm). (d) I_2/I_1 ratio against temperature for the 50 ppm of CDs in H_2O, DMF, and glycerol. PL spectra of 50 ppm of CDs in (e) H_2O, (f) DMF, and (g) glycerol at different temperatures, measured at 655 nm excitation. (h) Temperature dependence of the NIR emission intensity of 50 ppm of CDs in H_2O, DMF, and glycerol.

deprotonation of the CD surface results in increased PL intensity. A plausible energy structure of CDs depending on the protonation/deprotonation process is presented in Figure 4a. The excited state of the surface (S^*_{surf}) can be shifted to lower or higher energy during the protonation or deprotonation process, respectively.[18] During the CD surface deprotonation, the energy gap between the excited state of the core (S^*_{core}) and the excited states of the surface (which are related to the solvent change) decreases together with nonradiative energy dissipation, resulting in the increase of PLQY as was observed for CDs in aprotic solvents (Figure 3e).

At the same time, a clear trend of shifting the PL peak of CDs toward lower energies with increasing solvent polarity is observed in Figure 3d, which is different from an almost unchanged position of their absorption peak. This implies that the polarity of the solvent affects the lowest excited state from which the radiative recombination occurs, which is illustrated in the energy structure diagram presented in Figure 4b. After absorption of the photon, a rapid internal conversion occurs to the lowest excited energy state, S^*_{surf}. The excited state is then stabilized by the polar solvent molecules through reorientation of their dipoles and relaxation around the excited state, which

https://dx.doi.org/10.1021/acs.jpclett.0c03383
J. Phys. Chem. Lett. 2021, 12, 604–611

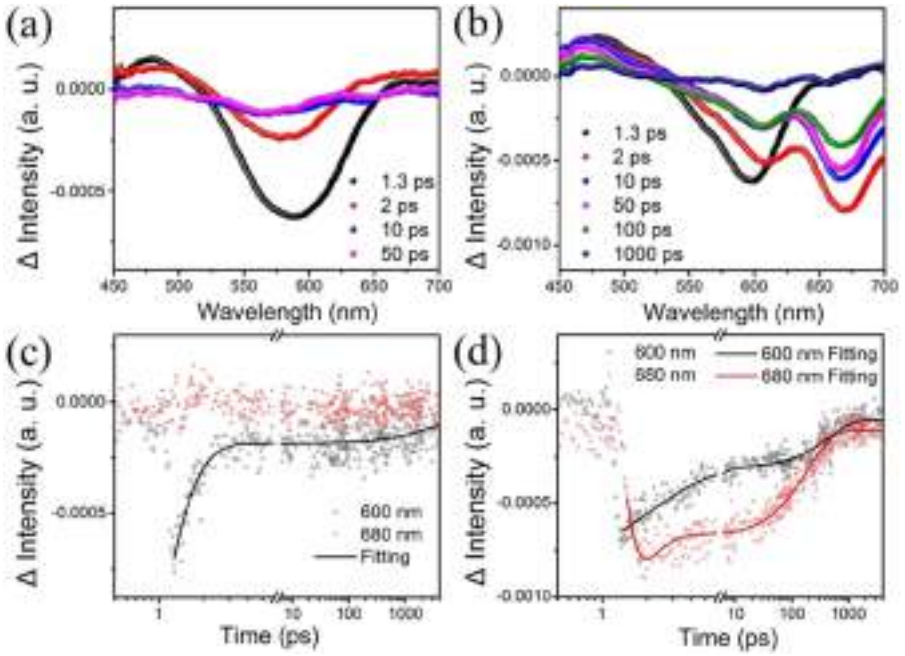

Figure 6. TA spectra of CDs in (a) H_2O and (b) DMF at indicated times delays, after excitation at λ_{pump} = 400 nm (1 kHz, 50 fs) with an excitation density of 5.0 μJ cm^{-2}. Bleach signal kinetics of the CDs in (c) H_2O and (d) DMF for λ_{pump} = 400 nm and probe wavelengths of 600 nm (black symbols/lines) and 680 nm (red symbols/lines). Dots are experimental points, and solid lines are fitting lines.

results in the decrease of the energy of the excited state (S^*_{surf}). With the increase of the solvent polarity, this effect becomes stronger, leading to the observation of the PL emission at lower energies.[18] Both PLQY and the average PL lifetime of CDs exhibit a linear dependence on the solvent polarity, as shown in Figure 3e. It is worth mentioning that for CDs in glycerol solution the PLQY breaks out from the above-mentioned linear dependence and is larger than expected according to the PL lifetime value. This observation can be explained by taking into account the large value of the glycerol viscosity (Table 1), which favors suppression of the vibrational motions and, hence, nonradiative losses in the sample. This results in the increase of the PLQY of CD in glycerol. Figure 3f shows the bright field and NIR images of the CDs in different solvents, which are well consistent with values of PLQY shown in Figure 3e.

Since the vibrations of surface groups of CDs, such as amine, carbonyl, and amide, and their interactions with solvent are sensitive to the temperature of the environment, temperature-dependent measurements of the absorption and NIR emission spectra of CDs in H_2O, glycerol, and DMF were carried out (Figure 5). For the CDs in H_2O, upon increasing the temperature from 10 to 80 °C, the absorption band I_1 at 605 nm gradually decreased, while the absorption band I_2 at 665 nm increased, which somewhat contradicts the common observation that the PL intensity tends to decrease at high temperatures.[19] The reason could be that the H-bonding between H_2O molecules and the surface carbonyl groups of CDs may become weakened at higher temperatures, leading to a lower degree of the protonation of the CD surface, which is then accompanied by an increase of the absorption band at 665 nm, and the related NIR emission at 705 nm. The I_2/I_1 ratio of the absorption peaks at 665 nm/605 nm is given in Figure 5d. For the CDs in DMF and glycerol solvents, the opposite effect is observed: the NIR emission intensity increased with decreasing the temperature (Figure 5h), accompanied by almost unchanged absorption (Figure 5d). It is worth mentioning that for CDs in glycerol solution, the main PL peak shifts from 705 to 685 nm upon decreasing temperature, which is accompanied by an almost 8-fold enhancement and appearance of the lower energy band in the emission spectrum, which then has a shape similar to that of CDs in protic solvents. These observations are correlated with those observed for organic fluorophores, whose emissions shift to shorter wavelengths with a temperature decrease.[18] At the same time, as at lower temperatures, the solvents become more viscous (Figure S1), the time for the solvent reorientation increases, and the rate K_S in Figure 4b decreases, which may also affect the energy structure of CDs. This effect is similar to the decrease of the solvent polarity, which is in agreement with changes of absorption and the PL peak positions shown in Figure 3d.

The excited-state dynamics of CDs interacting with different solvents were further investigated via transient absorption (TA) spectroscopy measurements performed under femtosecond pulse excitation at 400 nm. In aqueous solution, CDs exhibit a single ground-state bleach (GSB1) peak centered at 600 nm which is related to the I_1 absorption band (Figure 6a). Following the time profile at 600 nm, as shown in Figure 6c, this initially populated state—the excited state of the inner carbon core—deactivates rapidly within 1.54 ± 0.52 ps, and around 90% of its initial population depopulates through nonradiative relaxation, i.e., the vibrational motions. The weak long-lived state with a lifetime of 804.00 ± 247.71 ps is assigned to the excited state of the CD surface (I_2 absorption band). As for the CDs in DMF, as shown in Figure 6b, after the initial excitation of the CD inner core (GSB1 at 600 nm), a bleaching feature around 680 nm (GSB2) ascribed to CD surface state arises due to the energy transfer process from the excited state of the core (I_1 absorption band). This energy transfer process is rather fast, with a lifetime of 0.38 ± 0.01 ps. The bleaching feature of the inner carbon core (GSB1)

https://dx.doi.org/10.1021/acs.jpclett.0c03383
J. Phys. Chem. Lett. 2021, 12, 604−611

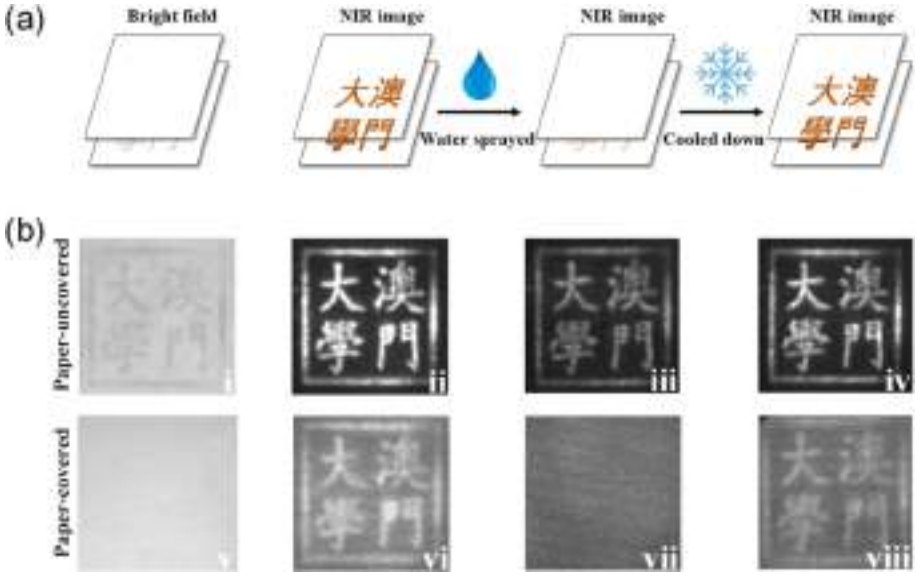

Figure 7. (a) Schematic diagram of the multilevel encryption system based on the CD ink. (b) Bright field (i and v) and NIR fluorescence images (ii–iv, vi–viii) of the CD pattern excited at 655 nm. Images were taken without (i–iv) and with (v–viii) cover paper.

deactivates to the ground state in 457.19 ± 185.23 ps, and to the surface state (GSB2) in 192.83 ± 9.12 ps, as shown in Figure 6d. The latter process corresponds to the enhanced NIR emission. The assignment of the GSB2 to the surface state agrees well with the steady-state spectral measurements shown in Figure 1a, Figure 3a, and Figure 5, since the absorption peak at 660–670 nm is highly sensitive to the chemical environment: H-bonding, protonation/deprotonation, and solvent polarity.

Energy diagrams summarizing the proposed mechanisms of the photophysical processes taking place in the CDs in aqueous and DMF solutions are presented in Figure 4c,d, respectively. In the aqueous solution, after the fast absorption to the excited core state (S^*_{core}), the energy rapidly dissipates to the ground state nonradiatively; only a small part of the energy transfers to the surface state (S^*_{surf}) followed by relaxation to the lowest energy state from which both radiative and nonradiative energy dissipations may occur. The radiative recombination is suppressed by vibrational motions and protonation of the CD surface. For the CDs in DMF solution, after absorption to the highest energy levels, the excitation undergoes a transfer to the S^*_{surf} energy level, and from there it dissipates to the lowest excited state, which lies slightly higher than that for the CDs in aqueous solution due to the lower polarity of DMF and its stronger deprotonation ability. From the lowest excited state, excitons relax radiatively giving rise to the NIR emission with almost 25-fold enhancement compared to that of the CD aqueous solution, which indicate strongly suppressed nonradiative relaxation.

The peculiar NIR emission properties of CDs in different solvents offer the possibility of their application in multilevel information encryption. Here, the CDs solution in glycerol was used as an ink to stamp luminescent patterns on a commercial printing paper to realize multiple luminescence-based encryptions, as illustrated in Figure 7a. As shown in Figure 7b, a luminescent pattern of the "University of Macau" in Chinese characters stamped by the CD ink can be observed under daylight but it naturally becomes completely invisible when covered with a printing paper. Under 655 nm excitation, the pattern can be easily observed through the cover paper, which is due to the efficient penetration of NIR emission from the CD ink, which constitutes the first level of the encryption. After spraying water on the patterned paper (Figure 7b-iii and Figure 7b-vii), the NIR emission from the pattern is significantly weakened and cannot be detected through the cover paper, which is due to the quenching of CD NIR emission by H_2O. The NIR emission of the CD pattern sensitive to humidity can be encrypted on the second level. First, as demonstrated above, lowering the temperature can increase the viscosity of glycerol and increase the NIR emission intensity. To prove this, the CD-ink stamped paper was moved to a refrigerator and held at −20 °C for 10 min, after which the pattern could be again recognized through the cover paper, as shown in Figure 7b-iv and Figure 7b-viii. This is the second level of the encryption. Thus, multilevel data encryption based on the adjustable NIR emission of CDs by controlling humidity and temperature of the environment has been realized.

In summary, we developed a simple and effective method to significantly enhance both the absorption and emission of CDs in the deep-red/NIR region by suppressing nonradiative charge recombination via deprotonation of the CD surface, which has been accomplished by changing the solvent deprotonation ability and viscosity. The absorption band at 630–700 nm increased, and the PLQY of the NIR emission reached 4% and 6% for CDs dissolved in glycerol and DMSO solutions at room temperature, respectively, which is a large improvement compared to only 0.2% PLQY in aqueous solution. The temperature decrease led to further enhancement of the NIR emission due to the increased viscosity of the solvent, which resulted in lowering energy losses at the CD surface. As compared with CD aqueous solutions at room temperature, the intensity of the NIR emission of CDs in DMF and glycerol solutions at −20 °C increased 50- and 70-fold, respectively. In our spectroscopy data analysis, we ascribe absorption bands at 520–630 and 630–700 nm as belonging to the CD inner core state and surface state, respectively, with the main contribution to the NIR emission coming from the surface state. On the basis of the changes of the NIR emission of CDs determined by changing environment, multilevel

https://dx.doi.org/10.1021/acs.jpclett.0c03383
J. Phys. Chem. Lett. 2021, 12, 604–611

fluorescence encryption was realized by varying humidity and temperature of the CD-ink stamped paper. Our study opens up a facile route to enhancement of the CD emission of CDs and provides a new prospect for future practical applications of CDs in data encryption.

CHEMICALS AND MATERIALS

Citric acid, urea, DMF, DMSO, ethanol, and glycerol were purchased from Aladdin. H_2O was deionized and purified on a Labconco WaterPros purification system. All reagents had at least analytical grade purity and were used as received without further purification.

SYNTHESIS OF CDS

First, citric acid (2 g) and urea (6 g) were reacted at 160 °C for 4 h under solvothermal conditions in 30 mL of DMSO and then cooled to room temperature. The acquired dark solution was mixed with twice its volume of ethanol and then centrifuged at 8000 r min^{-1} for 5 min. The precipitate was collected and freeze-dried.

CHARACTERIZATION

UV−vis absorption spectra were collected on a Shimadzu UV-2600 spectrophotometer. Steady-state PL spectra were measured on an Ocean Optics QE pro, and time-resolved PL spectra, on a LifeSpec-II lifetime spectrometer (Edinburgh Instruments). FT-IR spectra were performed on a Bruker Tensor 27 FT-IR spectrometer. TA measurements were performed on an Ultrafast System HELIOS spectrometer in a nondegenerate pump−probe configuration. The laser source was the Coherent Legend regenerative amplifier (100 fs, 1 kHz, 400 nm) seeded by a Coherent Vitesse oscillator (100 fs, 80 MHz). The pH values of the CD aqueous solutions were adjusted with HCl or NaOH aqueous solution by precise pH Meter (PHS-25, China). The viscosity data of all solvents was collected on a Discovery HR-2 hybrid rheometer. The photoluminescence quantum yield of all nanomaterials was collected at room temperature on an Edinburgh FS5 spectrophotometer.

ASSOCIATED CONTENT

Supporting Information

The Supporting Information is available free of charge at https://pubs.acs.org/doi/10.1021/acs.jpclett.0c03383.

Viscosity evolutions (PDF)

AUTHOR INFORMATION

Corresponding Authors

Songnan Qu − *Joint Key Laboratory of the Ministry of Education, Institute of Applied Physics and Materials Engineering, University of Macau, Taipa 999078, Macau SAR;* orcid.org/0000-0003-4159-096X; Email: songnanqu@um.edu.mo

Zikang Tang − *Joint Key Laboratory of the Ministry of Education, Institute of Applied Physics and Materials Engineering, University of Macau, Taipa 999078, Macau SAR;* Email: zktang@um.edu.mo

Authors

Enshan Liu − *Joint Key Laboratory of the Ministry of Education, Institute of Applied Physics and Materials Engineering, University of Macau, Taipa 999078, Macau SAR*

Tao Liang − *Joint Key Laboratory of the Ministry of Education, Institute of Applied Physics and Materials Engineering, University of Macau, Taipa 999078, Macau SAR*

Elena V. Ushakova − *Department of Materials Science and Engineering and Centre for Functional Photonics (CFP), City University of Hong Kong, Kowloon 999077, Hong Kong SAR; Center of Information Optical Technologies, ITMO University, Saint Petersburg 197101, Russia;* orcid.org/0000-0001-6841-6975

Bingzhe Wang − *Joint Key Laboratory of the Ministry of Education, Institute of Applied Physics and Materials Engineering, University of Macau, Taipa 999078, Macau SAR*

Bohan Zhang − *Joint Key Laboratory of the Ministry of Education, Institute of Applied Physics and Materials Engineering, University of Macau, Taipa 999078, Macau SAR*

Huiqun Zhou − *State Key Laboratory of Quality Research in Chinese Medicine, Institute of Chinese Medical Sciences, University of Macau, Taipa 999078, Macau SAR*

Guichuan Xing − *Joint Key Laboratory of the Ministry of Education, Institute of Applied Physics and Materials Engineering, University of Macau, Taipa 999078, Macau SAR;* orcid.org/0000-0003-2769-8659

Chunming Wang − *State Key Laboratory of Quality Research in Chinese Medicine, Institute of Chinese Medical Sciences, University of Macau, Taipa 999078, Macau SAR*

Andrey L. Rogach − *Department of Materials Science and Engineering and Centre for Functional Photonics (CFP) and Shenzhen Research Institute, City University of Hong Kong, Kowloon 999077, Hong Kong SAR;* orcid.org/0000-0002-8263-8141

Complete contact information is available at: https://pubs.acs.org/10.1021/acs.jpclett.0c03383

Author Contributions

#E. S. Liu and T. Liang contributed equally to this work.

Author Contributions

S. N. Qu designed the experiments. E. S. Liu and T. Liang performed the synthesis and characterizations. B. Z. Wang performed the transient absorption measurements. S. N. Qu, Z. K. Tang, G. C. Xing, E. S. Liu, E. V. Ushakova, H. Q. Zhou, B. H. Zhang and C. M. Wang participated in the data analysis. E. S. Liu, T. Liang, S. N. Qu, E. V. Ushakova, B. Z. Wang, and A. L. Rogach wrote the paper. All authors contributed to the manuscript.

Notes

The authors declare no competing financial interest.

ACKNOWLEDGMENTS

This work was supported by the National Natural Science Foundation of China (61922091 and 91733302), the Science and Technology Development Fund, Macau SAR (0040/2019/A1, 0073/2019/AMJ, FDCT/199/2017/A3, and FDCT/013/2017/AMJ), the Fund from the University of Macau (SRG2019-00163-IAPME), the Research and Development Grant for Chair Professor Fund from the University of Macau (CPG2020-00026-IAPME), Research Grant (MYRG2019-00103-IAPME) from the University of Macau,

the Ministry of Science and Higher Education of the Russian Federation (Grant 14.Y26.31.0028), the RFBR Project No. 18-29-19122 mk, the Research Grant Council of Hong Kong S.A.R. (CityU 11306619), and the Science Technology and Innovation Committee of Shenzhen Municipality (JCYJ20190808181201899).

REFERENCES

(1) Feng, T.; Tao, S.; Yue, D.; Zeng, Q.; Chen, W.; Yang, B. Recent Advances in Energy Conversion Applications of Carbon Dots: from Optoelectronic Devices to Electrocatalysis. *Small* **2020**, *16*, 2001295.
(2) Zhou, Y.; Zahran, E. M.; Quiroga, B. A.; Perez, J.; Mintz, K. J.; Peng, Z.; Liyanage, P. Y.; Pandey, R. R.; Chusuei, C. C.; Leblanc, R. M. Size-dependent Photocatalytic Activity of Carbon Dots with Surface-state Determined Photoluminescence. *Appl. Catal., B* **2019**, *248*, 157−166.
(3) Li, S.; Su, W.; Wu, H.; Yuan, T.; Yuan, C.; Liu, J.; Deng, G.; Gao, X.; Chen, Z.; Bao, Y.; et al. Targeted Tumour Theranostics in Mice via Carbon Quantum Dots Structurally Mimicking Large Amino Acids. *Nat. Biomed. Eng.* **2020**, *4*, 704−716.
(4) Liu, H.; Sun, Y.; Yang, J.; Hu, Y.; Yang, R.; Li, Z.; Qu, L.; Lin, Y. High Performance Fluorescence Biosensing of Cysteine in Human Serum with Superior Specificity Based on Carbon Dots and Cobalt-derived Recognition. *Sens. Actuators, B* **2019**, *280*, 62−68.
(5) Bao, X.; Yuan, Y.; Chen, J.; Zhang, B.; Li, D.; Zhou, D.; Jing, P.; Xu, G.; Wang, Y.; Holá, K.; et al. In Vivo Theranostics with Near-infrared-emitting Carbon Dots-Highly Efficient Photothermal Therapy Based on Passive Targeting after Intravenous Administration. *Light: Sci. Appl.* **2018**, *7*, 91.
(6) Liu, J.; Geng, Y.; Li, D.; Yao, H.; Huo, Z.; Li, Y.; Zhang, K.; Zhu, S.; Wei, H.; Xu, W.; et al. Deep Red Emissive Carbonized Polymer Dots with Unprecedented Narrow Full Width at Half Maximum. *Adv. Mater.* **2020**, *32*, 1906641.
(7) Ding, H.; Wei, J.-S.; Zhong, N.; Gao, Q.-Y.; Xiong, H.-M. Highly Efficient Red-Emitting Carbon Dots with Gram-Scale Yield for Bioimaging. *Langmuir* **2017**, *33*, 12635−12642.
(8) Lu, S.; Sui, L.; Liu, J.; Zhu, S.; Chen, A.; Jin, M.; Yang, B. Near-Infrared Photoluminescent Polymer-Carbon Nanodots with Two-Photon Fluorescence. *Adv. Mater.* **2017**, *29*, 1603443.
(9) Wang, B.; Li, J.; Tang, Z.; Yang, B.; Lu, S. Near-infrared Emissive Carbon Dots with 33.96% Emission in Aqueous Solution for Cellular Sensing and Light-Emitting Diodes. *Sci. Bull.* **2019**, *64*, 1285−1292.
(10) Jiang, L.; Ding, H.; Xu, M.; Hu, X.; Li, S.; Zhang, M.; Zhang, Q.; Wang, Q.; Lu, S.; Tian, Y.; et al. UV-Vis-NIR Full-Range Responsive Carbon Dots with Large Multiphoton Absorption Cross Sections and Deep-Red Fluorescence at Nucleoli and in Vivo. *Small* **2020**, *16*, 2000680.
(11) Chao, D.; Lyu, W.; Liu, Y.; Zhou, L.; Zhang, Q.; Deng, R.; Zhang, H. Solvent-dependent Carbon Dots and Their Applications in the Detection of Water in Organic Solvents. *J. Mater. Chem. C* **2018**, *6*, 7527−7532.
(12) Tian, Z.; Zhang, X.; Li, D.; Zhou, D.; Jing, P.; Shen, D.; Qu, S.; Zboril, R.; Rogach, A. L. Full-Color Inorganic Carbon Dot Phosphors for White-Light-Emitting Diodes. *Adv. Opt. Mater.* **2017**, *5*, 1700416.
(13) Li, D.; Jing, P.; Sun, L.; An, Y.; Shan, X.; Lu, X.; Zhou, D.; Han, D.; Shen, D.; Zhai, Y.; et al. Near-Infrared Excitation/Emission and Multiphoton-Induced Fluorescence of Carbon Dots. *Adv. Mater.* **2018**, *30*, 1705913.
(14) Ding, H.; Wei, J.-S.; Zhang, P.; Zhou, Z.-Y.; Gao, Q.-Y.; Xiong, H.-M. Solvent-Controlled Synthesis of Highly Luminescent Carbon Dots with a Wide Color Gamut and Narrowed Emission Peak Widths. *Small* **2018**, *14*, 1800612.
(15) Li, Y.; Bai, G.; Zeng, S.; Hao, J. Theranostic Carbon Dots with Innovative NIR-II Emission for in Vivo Renal-Excreted Optical Imaging and Photothermal Therapy. *ACS Appl. Mater. Interfaces* **2019**, *11*, 4737−4744.
(16) Liu, K.-K.; Song, S.-Y.; Sui, L.-Z.; Wu, S.-X.; Jing, P.-T.; Wang, R.-Q.; Li, Q.-Y.; Wu, G.-R.; Zhang, Z.-Z.; Yuan, K.-J.; et al. Efficient Red/Near-Infrared-Emissive Carbon Nanodots with Multiphoton Excited Upconversion Fluorescence. *Adv. Sci.* **2019**, *6*, 1900766.
(17) Stepanidenko, E. A.; Arefina, I. A.; Khavlyuk, P. D.; Dubavik, A.; Bogdanov, K. V.; Bondarenko, D. P.; Cherevkov, S. A.; Kundelev, E. V.; Fedorov, A. V.; Baranov, A. V.; et al. Influence of the Solvent Environment on Luminescent Centers within Carbon Dots. *Nanoscale* **2020**, *12*, 602−609.
(18) Lakowicz, Joseph R. *Principles of Fluorescence Spectroscopy*; Springer: New York, 2006.
(19) Song, Y.; Zhu, S.; Xiang, S.; Zhao, X.; Zhang, J.; Zhang, H.; Fu, Y.; Yang, B. Investigation into the Fluorescence Quenching Behaviors and Applications of Carbon Dots. *Nanoscale* **2014**, *6*, 4676−4682.

https://dx.doi.org/10.1021/acs.jpclett.0c03383
J. Phys. Chem. Lett. 2021, 12, 604−611